nature neuroscience

VTA CRF neurons mediate the aversive effects of nicotine withdrawal and promote intake escalation

Taryn E Grieder[1], Melissa A Herman[2], Candice Contet[2], Laura A Tan[3], Hector Vargas-Perez[1], Ami Cohen[2], Michal Chwalek[1], Geith Maal-Bared[1], John Freiling[2], Joel E Schlosburg[2], Laura Clarke[1], Elena Crawford[2], Pascale Koebel[4], Vez Repunte-Canonigo[5], Pietro P Sanna[5], Andrew R Tapper[6], Marisa Roberto[2], Brigitte L Kieffer[4,7], Paul E Sawchenko[3], George F Koob[8], Derek van der Kooy[1] & Olivier George[2]

Dopaminergic neurons in the ventral tegmental area (VTA) are well known for mediating the positive reinforcing effects of drugs of abuse. Here we identify in rodents and humans a population of VTA dopaminergic neurons expressing corticotropin-releasing factor (CRF). We provide further evidence in rodents that chronic nicotine exposure upregulates *Crh* mRNA (encoding CRF) in dopaminergic neurons of the posterior VTA, activates local CRF_1 receptors and blocks nicotine-induced activation of transient GABAergic input to dopaminergic neurons. Local downregulation of *Crh* mRNA and specific pharmacological blockade of CRF_1 receptors in the VTA reversed the effect of nicotine on GABAergic input to dopaminergic neurons, prevented the aversive effects of nicotine withdrawal and limited the escalation of nicotine intake. These results link the brain reward and stress systems in the same brain region to signaling of the negative motivational effects of nicotine withdrawal.

Drug addiction has been hypothesized to be driven by two mechanisms: reduction of the activity of the brain reward system[1] and enhanced function of the anti-reward brain stress system[2], concepts known as within-system and between-systems neuroadaptations, respectively[3]. Prominent downregulation of the mesolimbic dopamine (DA) reward system originating in the ventral tegmental area (VTA) and upregulation of the CRF (also known as corticotropin-releasing hormone, CRH) brain stress system originating in the extended amygdala have been observed in rodents, nonhuman primates and humans during abstinence from drugs of abuse, including tobacco[4,5].

The VTA is a critical region for nicotine dependence[6], and several groups have examined the mechanisms behind DA and CRF neuroadaptations[7–13]. However, most of these studies were performed in nondependent animals, and these studies postulated that VTA CRF is released from axons that originate in the forebrain and not from local CRF neurons[7–13]. Thus, how the VTA DA and CRF systems interact in nicotine dependence and withdrawal is essentially unknown. Here we identify in rodents and humans a new population of CRF neurons in the VTA and demonstrate that recruitment of these CRF neurons in the VTA after chronic nicotine contributes to a within-system neuroadaptation of DA neurons to mediate the negative motivational state elicited by nicotine withdrawal.

RESULTS

Nicotine dependence upregulates *Crh* mRNA in the pVTA

To test whether nicotine dependence upregulates CRF in the brain stress and reward systems, we first measured *Crh* mRNA in two key regions of the CRF brain stress system, the paraventricular nucleus of the hypothalamus (PVN) and central nucleus of the amygdala (CeA), as well as in the VTA, using quantitative real-time (RT)-PCR. Groups of mice were made nicotine dependent by chronic exposure to nicotine delivered by osmotic minipumps (7 mg per kilogram body weight per day)[14,15]. Brain punches of the PVN, CeA and VTA (**Fig. 1a**) were sampled in saline-treated mice, dependent mice with nicotine minipumps or withdrawn mice (8 h after removal of the minipump)[14]. We consistently detected low levels of *Crh* mRNA in the VTA in saline-treated mice. *Crh* mRNA levels in the VTA were lower than in the CeA and PVN (VTA ranges 6–14% of CeA and PVN, $F_{2,33} = 4.9$, $P = 0.014$, **Supplementary Fig. 1**), in accordance with the fact that the CeA and PVN contain large populations of cell bodies that express *Crh* mRNA, whereas similar neurons have not been reported in the VTA[16] until now. Chronic exposure to nicotine increased *Crh* mRNA in the VTA in both the dependent and withdrawn groups of mice ($F_{2,100} = 2.7$, $P = 0.034$), without altering *Crh* expression in the PVN or CeA (**Fig. 1b**). Considering that CRF neurons in the CeA and PVN project to and synapse with both DA and GABA neurons in the VTA[17] and that CRF

[1]Institute of Medical Science and Department of Molecular Genetics, University of Toronto, Toronto, Ontario, Canada. [2]Committee on the Neurobiology of Addictive Disorders, The Scripps Research Institute, La Jolla, California, USA. [3]The Salk Institute, La Jolla, California, USA. [4]Institut de Génétique et de Biologie Moléculaire et Cellulaire, CNRS / INSERM / Université de Strasbourg, Illkirch, France. [5]Molecular and Cellular Neuroscience, The Scripps Research Institute, La Jolla, California, USA. [6]Brudnick Neuropsychiatric Research Institute, University of Massachusetts Medical School, Worcester, Massachusetts, USA. [7]Douglas Hospital Research Center, Department of Psychiatry, McGill University, Montreal, Quebec, Canada. [8]National Institute on Alcohol Abuse and Alcoholism, Rockville, Maryland, USA. Correspondence should be addressed to O.G. (ogeorge@scripps.edu).

Received 22 July; accepted 17 October; published online 17 November 2014; doi:10.1038/nn.3872

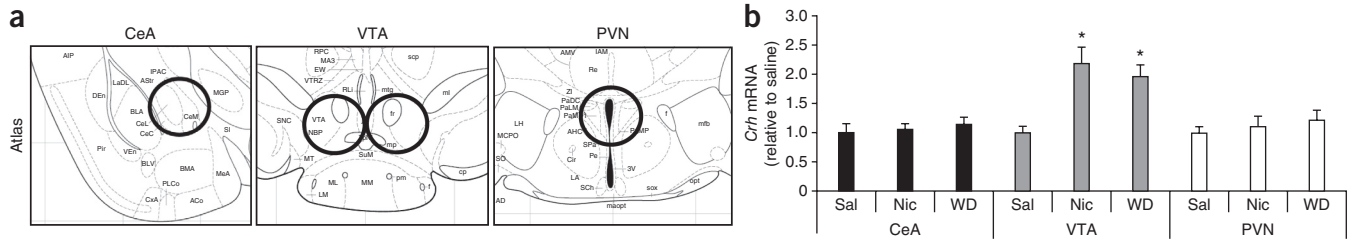

Figure 1 Nicotine dependence increases *Crh* mRNA in the VTA. (**a**) Locations of the brain tissue samples in the CeA, VTA and PVN. (**b**) *Crh* mRNA levels (ΔC_t) in the CeA, VTA and PVN relative to the housekeeping gene *Gapdh*, normalized to the saline group value in mice chronically exposed to saline (Sal) or nicotine (Nic) or withdrawn from chronic nicotine (WD) as measured by RT-PCR ($n = 13$ or 14 per group). A significant change in *Crh* mRNA was observed in the VTA but not CeA or PVN in both the Nic and WD groups (*$P < 0.05$ versus Sal). Data represent mean + s.e.m.

release in the VTA is potentiated after repeated but not acute cocaine exposure[8], the increase in *Crh* mRNA in the VTA observed herein could originate from either axonal transport of *Crh* mRNA to the VTA or the synthesis of *Crh* mRNA in local VTA neurons.

Identification of CRF neurons in the posterior VTA

To test the hypothesis that *Crh* mRNA is synthesized locally in the VTA, we performed *in situ* hybridization (ISH) for *Crh* mRNA in a separate cohort of mice that were drug naive or treated with acute nicotine (1.5 mg kg^{-1}), chronic nicotine (7 mg kg^{-1} d^{-1} for 12 d), or chronic nicotine and withdrawal (8 h). A population of CRF neurons with dense *Crh* mRNA in cell bodies could be detected bilaterally in the VTA in all groups, with most neurons located in the posterior VTA (pVTA), dorsal to the interpeduncular nucleus (IPN) (**Fig. 2**). No significant difference in the number of neurons was observed between groups ($F_{24,180} = 0.82$, $P = 0.71$, **Supplementary Fig. 2**), demonstrating that the increase in *Crh* mRNA was attributable to an increase in the production of *Crh* in individual neurons and not to an increase in the number of CRF neurons. To confirm the specificity of the *Crh* mRNA ISH, we performed urocortin (*Ucn*) mRNA ISH on adjacent sections. Urocortin is a structurally related peptide of the CRF family with affinity for the CRF_2 receptor[18]. No urocortin-positive neurons were observed in the VTA (**Supplementary Fig. 3**), whereas numerous urocortin-positive neurons were observed in the Edinger-Westphal nucleus (**Supplementary Fig. 3**), an area that is known to contain a large population of urocortin neurons[18]. Complementing these results, a recent study demonstrated that nicotine selectively activates DA neurons in the pVTA but not anterior VTA (aVTA), suggesting that CRF-expressing neurons in the pVTA may be dopaminergic[19]. To test this hypothesis, we then examined coexpression in VTA of *Crh* and tyrosine hydroxylase (TH), a marker for DA neurons in both mice and humans.

Crh mRNA is expressed in DA neurons

We performed double labeling for *Crh* mRNA and DA neurons using *Crh* mRNA radioactive ISH (**Fig. 3a**) and fluorescence ISH coupled with TH immunohistochemistry (**Fig. 3c,d**) in mice. *Crh* mRNA–positive neurons were located bilaterally in the VTA in TH-enriched regions (**Fig. 3b**), and 95.2 ± 4.8% of them expressed TH as well (**Fig. 3c,d**). To further confirm the existence of VTA CRF/DA neurons and test their relevance to humans, we performed *CRH* chromogenic ISH coupled with TH immunohistochemistry in VTA samples from three humans who were nonsmokers without any psychiatric disorders (see **Supplementary Table 1** for details). Of 600 CRF neurons, we found that 97.8 ± 0.7% were DA neurons (**Fig. 4**), confirming the existence of VTA CRF/DA neurons in both rodents and humans.

Withdrawal-induced CRF peptide depletion in the pVTA and IPN

Increased CRF release during drug withdrawal is associated with decreased immunodensity of CRF peptide in neuropils. The decrease in CRF immunodensity reflects CRF depletion from synaptic vesicles subsequent to a local increase in CRF release[20,21]. We thus used CRF immunohistochemistry to examine whether the recruitment of CRF neurons in the pVTA is also associated with a local decrease in CRF peptide density in neuropils during withdrawal from chronic nicotine. Densitometry revealed that both nicotine dependence and withdrawal from chronic nicotine decreased CRF peptide density as compared with that in saline-treated mice in the pVTA ($F_{2,31} = 4.40$, $P = 0.02$; **Supplementary Fig. 4a**), IPN ($F_{2,49} = 4.24$, $P = 0.020$; **Supplementary Fig. 4d**) and CeA ($F_{2,67} = 3.15$, $P = 0.049$; **Supplementary Fig. 4c**) but not aVTA ($F_{2,23} = 0.03$, $P = 0.97$; **Supplementary Fig. 4a**) or PVN ($F_{2,21} = 0.75$, $P = 0.48$; **Supplementary Fig. 4b**), demonstrating the specificity of these effects. The combined observations that chronic nicotine exposure increased *Crh*

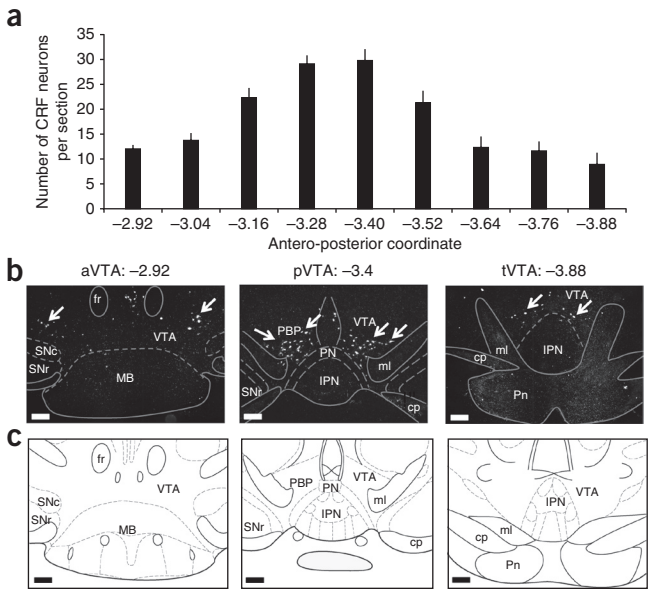

Figure 2 Identification of VTA CRF neurons in mice. (**a**) Number of CRF neurons per section in the VTA (–2.92 to –3.88 mm from bregma) in mice ($n = 24$ mice). Data represent mean + s.e.m. (**b**) Representative *Crh* mRNA *in situ* hybridization sections of the anterior (aVTA), posterior (pVTA) and tail (tVTA) in naive mice. White arrows point to CRF neurons. fr, fornix; SNC, substantia nigra pars compacta; SNr, substantia nigra pars reticulata; MB, mammillary body; PBP, parabrachial pigmented area; PN, paranigral nucleus; ml, median lemniscus; cp, cerebral peduncle; Pn, pontine nuclei. (**c**) Corresponding atlas diagram[50]. Scale bars, 200 μm.

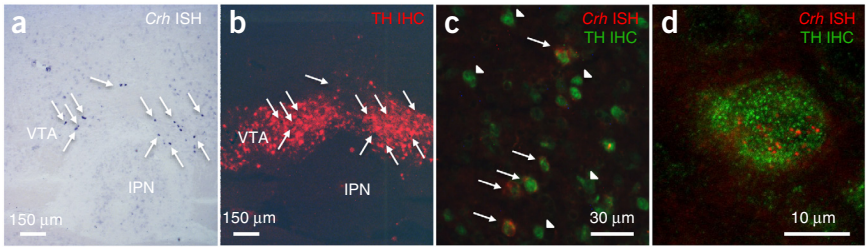

Figure 3 Double labeling of CRF/DA neurons using *Crh in situ* hybridization and TH immunohistochemistry in mice. (**a**) *Crh* mRNA radioactive *in situ* hybridization (black) demonstrating *Crh*-positive cell bodies (arrows) in the pVTA. (**b**) TH immunohistochemistry (red) on a neighboring section of the pVTA showing that dopaminergic cell bodies were located bilaterally in the pVTA in TH-immunoreactive areas. (**c**) Double fluorescence labeling of *Crh* mRNA (red) and TH protein (green) in the pVTA at high magnification. Fluorescence ISH is less sensitive than radioactive or chromogenic ISH; thus, a limited number of neurons expressing *Crh* mRNA could be identified in the pVTA in nicotine-dependent mice using this procedure. However, it served to achieve high-resolution imaging and assess the cellular colocalization of *Crh* mRNA with TH. Of 18 neurons that unambiguously expressed *Crh* mRNA, 16 were TH-positive (Crh^+ TH^+ neurons, arrows; Crh^- TH^+ neurons, arrowheads). (**d**) Confocal image of a single VTA neuron expressing both TH and *Crh* mRNA. Confocal analysis was repeated on 13 sections from three mice.

mRNA expression and decreased CRF peptide density in the pVTA and IPN suggest that CRF/DA neurons in the pVTA may release CRF locally in the pVTA and IPN during nicotine dependence. However, the possibility that CRF may also be released from extrinsic projection neurons, such as CRF neurons in the CeA, cannot be ruled out because decreased immunodensity was also observed in the CeA (**Supplementary Fig. 4c**). The decreased CRF immunodensity in the CeA replicates results obtained with alcohol-dependent rats[21] and extends this work to nicotine-dependent and nicotine-withdrawn mice.

pVTA *Crh* mRNA downregulation prevents nicotine dependence–induced dysregulation at GABA neuron–DA neuron synapses

The downregulation of VTA DA neuron activity is a key feature of addiction, and recent results have shown that nicotine-induced GABA currents are critical for the phasic activation of dopamine neurons[22]. To test whether *Crh* mRNA–expressing neurons in the pVTA exert synaptic control over DA neurons, we tested the causal relationship between downregulation of *Crh* mRNA in the pVTA of nicotine-dependent and nicotine-withdrawn mice and the effect of nicotine on GABAergic currents in DA neurons. Local downregulation of *Crh* mRNA was performed using an adeno-associated viral vector that encodes a short hairpin RNA targeting *Crh* mRNA (AAV2-shCRH) or a non-targeting sequence (AAV2-shSCR; **Supplementary Fig. 5a,b**). The AAV2-shCRH vector decreased the amount of *Crh* mRNA by 88.0 ± 6.2% as measured by RT-PCR on VTA punches ($t_{10} = 11.12$, $P = 0.0001$, $n = 6$ mice per condition). Some neurons exhibited an even stronger downregulation, having no detectable *Crh* mRNA remaining after treatment with the silencing vector, such that the total number of CRF-positive neurons decreased by 26% (**Supplementary Fig. 5c,d**).

We first performed whole-cell voltage-clamp recordings of pharmacologically isolated $GABA_A$ receptor–mediated spontaneous inhibitory postsynaptic currents (sIPSCs) in putative pVTA DA neurons from naive mice. Dopamine neurons were identified at the time of recording by previously published functional criteria[23,24] (**Supplementary Fig. 6**), and a subset of neurons was collected after recording for *Th* mRNA expression analysis using single-cell RT-PCR. To examine the effects of nicotine dependence on changes in GABAergic transmission in pVTA DA neurons with and without downregulation of *Crh* mRNA, neurons infected with either AAV2-shSCR or AAV2-shCRH were identified during withdrawal (6–8 h) by the presence of GFP in the cell body (**Fig. 5c**). In naive mice, acute application of nicotine

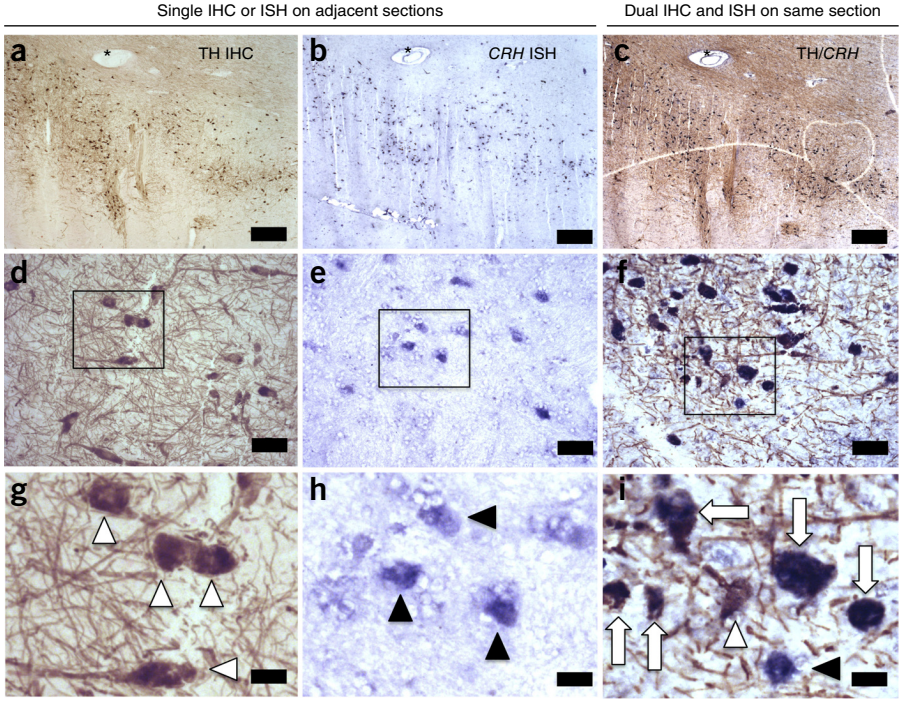

Figure 4 Double labeling of CRF/DA neurons using *CRH in situ* hybridization and TH immunohistochemistry in humans. Single TH immunohistochemistry (**a**,**d**,**g**, light brown) and *CRH* ISH (**b**,**e**,**h**, blue) were performed on different but adjacent sections (distance: 80 µm) of the VTA (human sample HSB3750). Note the similar distributions of TH (white arrowheads) and *CRH* (black arrowheads) within the VTA (use blood vessel marked with * as a landmark). Double TH immunochemistry and *CRH* ISH (**c**,**f**,**i**) were performed on a section adjacent to the corresponding single-stain sections; note blood vessel (*). White arrows point to colocalized TH and *CRH* in individual neurons. Very few neurons were single-labeled as TH-only (white arrowhead) and *CRH*-only (black arrowhead). This experiment was repeated on brain samples from three human subjects. Scale bars: 200 µm (**a**–**c**), 40 µm (**d**–**f**), 10 µm (**g**–**i**).

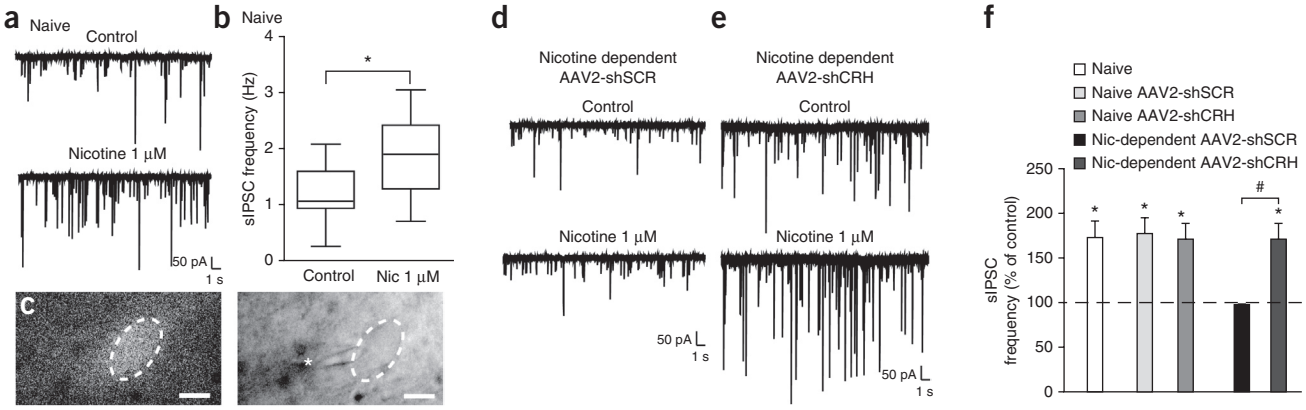

Figure 5 Nicotine dependence causes dysregulation of GABA-DA synapses, which is reversed by downregulation of *Crh* mRNA. (**a**) Representative voltage-clamp recording of sIPSCs in a pVTA DA neuron from a naive mouse before (control) and during the application of nicotine (1 μM). Centerline respresents the median; box limits, first and third quartiles; whiskers, lowest and highest values. (**b**) Box-and-whisker plot of average sIPSC frequency before (control) and during nicotine (Nic) application ($n = 8$ cells from three mice). $^{*}P = 0.0015$. (**c**) Photomicrograph at 60× magnification of a pVTA DA neuron from a nicotine-dependent mouse showing GFP fluorescence (left panel) and an infrared differential interference contrast image taken during recording (right panel; * marks the pipette). (**d**) Representative voltage-clamp recording of sIPSCs in a pVTA DA neuron from a nicotine-dependent mouse injected with AAV2-shSCR before (control) and during application of nicotine (1 μM). (**e**) Representative voltage-clamp recording of sIPSCs in a pVTA DA neuron from a nicotine-dependent mouse injected with AAV2-shCRH before (control) and during application of nicotine (1 μM). (**f**) Summary of average change in sIPSC frequency produced by nicotine in pVTA DA neurons from naive mice ($n = 8$ cells from three mice; $^{*}P = 0.01$), naive mice injected with either AAV2-shSCR ($n = 12$ cells from three mice; $^{*}P = 0.001$) or AAV2-shCRH ($n = 12$ cells from three mice; $^{*}P = 0.001$) and nicotine-dependent mice injected with either AAV2-shSCR ($n = 11$ cells from four mice; $P = 0.25$) or AAV2-shCRH ($n = 10$ cells from four mice; $^{*}P = 0.001$; $^{\#}P = 0.0003$ versus nicotine-dependent AAV2-shSCR). Data represent mean + s.e.m.

(1 μM) onto pVTA DA neurons produced a transient, significant increase in sIPSC frequency from 1.2 ± 0.2 Hz to 1.9 ± 0.3 Hz ($t_7 = 5.048$, $P = 0.0015$, paired t-test; **Fig. 5a,b**; 172.9 ± 18.5% of control, $t_7 = 3.93$, $P = 0.0057$, one-sample t-test; **Fig. 5f**), consistent with previous reports[25,26]. Nicotine also increased sIPSC frequency in pVTA DA neurons from mice implanted with saline minipumps and infected with AAV2-shSCR or AAV2-shCRH (176.9 ± 18.2% of baseline without nicotine; $t_{11} = 4.217$, $P = 0.0014$ and 171.5 ± 16.7% of baseline without nicotine; $t_{11} = 4.248$, $P = 0.0013$, respectively; **Fig. 5f**). In contrast, in pVTA DA neurons from nicotine-dependent mice injected with AAV2-shSCR, acute application of nicotine (1 μM) produced no change in sIPSC frequency (97.7 ± 1.8% of baseline without nicotine; $t_{10} = 1.228$, $P = 0.2474$; **Fig. 5d,f**), which was significantly different from the effects observed in naive mice or mice implanted with saline minipumps (one-way ANOVA, $F_{4,48} = 4.704$, $P = 0.0028$). However, during acute application of nicotine (1 μM) in pVTA DA neurons from nicotine-dependent mice injected with AAV2-shCRH, the nicotine-induced increase in sIPSC frequency was restored (171.2 ± 17.3% of baseline without nicotine; $t_9 = 4.108$, $P = 0.0026$, one-sample t-test; **Fig. 5e,f**), which was significantly different from that observed in pVTA DA neurons from nicotine-dependent mice injected with AAV2-shSCR (unpaired t-test; $t_{19} = 4.426$, $P = 0.0003$) but not different from that observed in naive mice. To confirm the identity of the putative DA neurons, we performed single-cell RT-PCR after recordings to detect the presence of *Th* mRNA. The majority (13 of 18; 72%) of the VTA cells examined by single-cell PCR were *Th*-positive, and the electrophysiological results were similar when only *Th*-positive neurons were included (**Supplementary Fig. 7**). Collectively, these data demonstrate that nicotine-induced activation of GABA neurons, a key mechanism required for DA neuron firing[22], is deficient in nicotine-dependent mice and that downregulation of *Crh* mRNA in the VTA can reverse the effect of nicotine dependence.

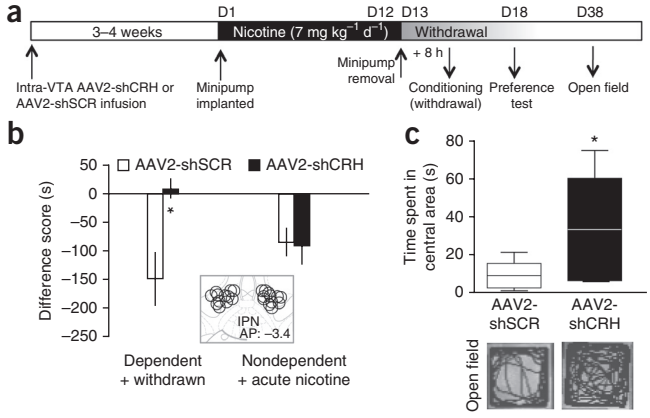

Figure 6 Viral vector–mediated downregulation of *Crh* mRNA in the VTA prevents the aversive motivational response to nicotine withdrawal. (**a**) Timeline of experiment. (**b**) Difference score (s) during testing of conditioned place aversion to nicotine withdrawal in nicotine-dependent and nicotine-withdrawn groups or a nondependent group given acute nicotine after AAV2-shSCR or AAV2-shCRH treatment ($n = 11$ mice per group). Mice infused with the silencing vector did not show the conditioned aversive motivational response (a negative difference score) to withdrawal from chronic nicotine ($^{*}P = 0.02$) that was observed in mice given the control vector. Nondependent mice given AAV2-shSCR or AAV2-shCRH showed an aversive response to acute nicotine. Data represent mean ± s.e.m. The inset shows the viral vector injection site; AP, antero-posterior coordinate in mm. (**c**) Box-and-whisker plot showing time spent in the central area of the open field in nicotine-dependent and nicotine-withdrawn mice injected with AAV2-shSCR ($n = 8$) or AAV2-shCRH in the VTA ($n = 8$; $^{*}P < 0.05$). Centerline respresents the median; box limits, first and third quartiles; whiskers, lowest and highest values. Pictures below are example traces showing activity patterns in the open field of a mouse injected with the corresponding vector. See **Supplementary Figure 5** for details on the viral vector.

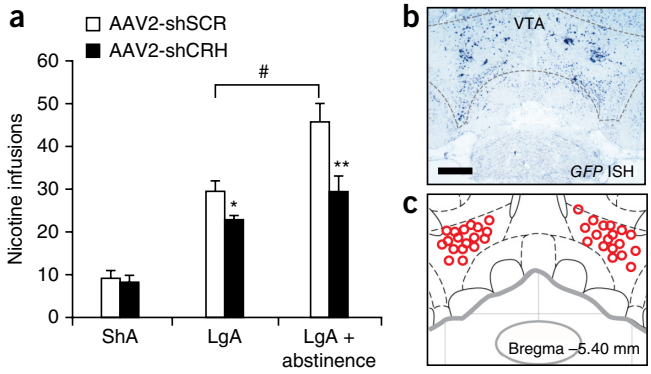

Figure 7 Viral vector-mediated downregulation of *Crh* mRNA in the VTA decreases long-access nicotine self-administration and prevents abstinence-induced escalation of nicotine intake. (**a**) Number of nicotine self-administrations in rats injected with AAV2-shSCR or AAV2-shCRH and given short access (1 h d^{-1} for 10 d; AAV2-shCRH, $n = 9$; AAV2-shSCR, $n = 9$), long access (21 h d^{-1} for 7 d; AAV2-shCRH, $n = 8$; AAV2-shSCR, $n = 7$) or long access after 48 h of abstinence (LgA + abstinence; $n = 11$) to nicotine. AAV2-shCRH reduced the number of nicotine infusions in the LgA group (*$P = 0.018$ versus AAV2-shSCR) and LgA + abstinence group (**$P = 0.004$ versus AAV2-shSCR). Comparisons of the AAV2-shSCR LgA groups before and after abstinence with regard to the number of infusions after abstinence demonstrate the abstinence-induced escalation of nicotine intake ($^{\#}P = 0.008$). Data represent mean + s.e.m. (**b**) Representative section from an AAV2-shCRH-injected mouse showing *GFP* ISH (dark blue). Scale bar, 400 µm. (**c**) Viral vector injection site.

pVTA *Crh* mRNA downregulation prevents the aversive effects of nicotine withdrawal

To test whether *Crh* mRNA–expressing neurons in the pVTA affect the motivational effects of nicotine dependence, we examined the causal relationship between downregulation of *Crh* mRNA in the pVTA of nicotine-dependent and nicotine-withdrawn mice and the expression of conditioned place aversion to nicotine withdrawal and anxiety-like behavior (**Fig. 6a**). In the place-conditioning procedure, a two-way ANOVA revealed a significant interaction between AAV2 injection and nicotine history ($F_{1,40} = 5.80$, $P = 0.021$; **Fig. 6b**). Nicotine-dependent and nicotine-withdrawn mice infused with the AAV2-shSCR control vector in the pVTA showed an aversive motivational response to the withdrawal-paired environment ($P = 0.032$), which was not observed in mice infused with the AAV2-shCRH vector ($P = 0.6392$). Mice that were injected with the AAV2-shCRH vector outside the pVTA (mostly located dorsal or lateral to the pVTA, in the red nucleus or substantia nigra, respectively) showed an aversive response to nicotine withdrawal like that of control mice (unpaired *t*-test; $t_{16} = 0.0255$, $P = 0.798$; **Supplementary Fig. 8**), demonstrating the anatomical specificity of this effect. Furthermore, nondependent mice given either the AAV2-shSCR or AAV2-shCRH vector in the pVTA and an acute injection of nicotine (1.75 mg kg^{-1}), known to be aversive[14,15], showed an aversive response to the nicotine-paired environment (**Fig. 6b**), demonstrating that the lack of aversion to withdrawal in dependent mice infused with the silencing vector was not attributable to a general impairment of conditioned place aversion, but was specific to nicotine withdrawal in dependent mice. Taken together, these results suggest that *Crh* mRNA in the pVTA does not mediate a general aversive response to acute nicotine but specifically mediates aversion to nicotine withdrawal in dependent subjects. These results establish a causal relationship between the recruitment of *Crh* mRNA–expressing neurons in the pVTA during withdrawal from chronic nicotine and the aversive motivational response to nicotine withdrawal.

Activation of the brain CRF-CRF_1 receptor system is associated with increased anxiety-like behavior in humans and animals and is hypothesized to be responsible for the negative emotional state after protracted abstinence[27]. To test this hypothesis, we measured open field activity to evaluate anxiety-like behavior during protracted abstinence (3–4 weeks). Mice injected with the AAV2-shSCR vector spent significantly less time in the central area of the open field than mice injected with the AAV2-shCRH vector (unpaired *t*-test; $t_{14} = 2.84$, $P = 0.013$; **Fig. 6c**), an effect that was not attributable to a decrease in locomotion (AAV2-shSCR, 2,181 ± 215 cm; AAV2-shCRH, 2,307 ± 146 cm; $t_{14} = 0.49$, $P = 0.64$). These results demonstrate that upregulation of *Crh* mRNA in the pVTA is required for the anxiogenic-like effects of protracted nicotine abstinence.

pVTA *Crh* mRNA downregulation decreases abstinence-induced escalation of nicotine intake

To test whether *Crh* mRNA–expressing neurons in the pVTA influence the motivation to take nicotine during abstinence, we infused the same AAV2-shCRH or AAV2-shSCR vectors into the pVTAs of rats and measured nicotine self-administration 4 weeks later. In rats given short access (1 h d^{-1}) to nicotine self-administration for 10 d, downregulation of *Crh* mRNA in the VTA did not affect nicotine intake (unpaired *t*-test; $t_{17} = 0.59$, $P = 0.28$; **Fig. 7**). We then gave the rats long access (21 h d^{-1}) to nicotine self-administration and measured nicotine intake after 7 d of long access and after 48 h of abstinence[27–29]. Infusion of AAV2-shCRH decreased nicotine intake in long-access rats (unpaired *t*-test; $t_{14} = 2.32$, $P = 0.018$) and prevented abstinence-induced increases in nicotine intake, whereas the rats that received AAV2-shSCR showed a significant increase in nicotine intake after 48 h of abstinence ($F_{1,14} = 4.91$, $P = 0.044$; **Fig. 7**). These results demonstrate that pVTA *Crh* mRNA downregulation decreases excessive nicotine intake and is particularly effective at decreasing the abstinence-induced escalation of nicotine intake.

Blocking CRF_1 receptors prevents the aversive effect of nicotine withdrawal

The present results revealed a depletion of CRF peptide in the pVTA during nicotine withdrawal, hypothesized to reflect a local increase in CRF release[20,21]. To further test this hypothesis, we examined whether the activation of CRF_1 receptors in the pVTA is necessary for the conditioned aversive motivational response to a withdrawal-paired environment shown by nicotine-dependent and nicotine-withdrawn mice[14,15]. We administered the CRF_1 receptor antagonist *N*,*N*-bis(2-methoxyethyl)-3-(4-methoxy-2-methylphenyl)-2,5-dimethyl-pyrazolo[1,5-a]pyrimidin-7-amine (MPZP; 20 mg kg^{-1}, subcutaneously)[27] before place conditioning in nondependent mice given acute nicotine, nicotine-dependent mice with minipumps (7 mg kg^{-1} d^{-1}) or mice in spontaneous withdrawal (8 h) from chronic nicotine (**Fig. 8a**). A two-way ANOVA showed a significant effect of systemic MPZP treatment ($F_{3,103} = 20.51$, $P < 0.0001$; **Fig. 8b**). Withdrawn mice pretreated with vehicle showed a conditioned place aversion to a withdrawal-paired environment that was blocked by MPZP ($P = 0.0043$), demonstrating that activation of CRF_1 receptors during withdrawal is required for the aversive motivational response to nicotine withdrawal. Nicotine-dependent mice that were not in withdrawal and were pretreated with saline showed a conditioned place preference for the nicotine-paired environment that was not blocked by MPZP pretreatment ($P = 0.9085$). These results suggest that the activation of CRF_1 receptors is not required for the rewarding motivational response to chronic nicotine in dependent mice.

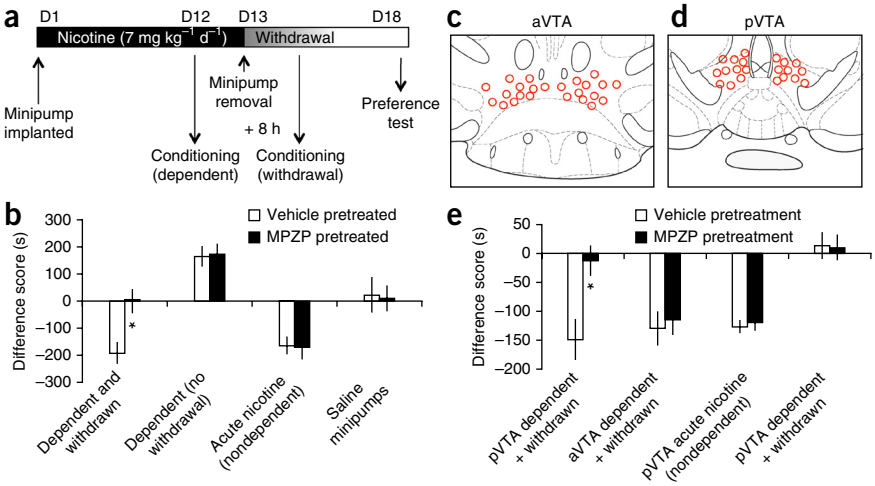

Figure 8 CRF_1 receptor antagonism prevents the aversive motivational response to withdrawal from chronic nicotine. (**a**) Timeline of experiment. (**b**) Nicotine-dependent and nicotine-withdrawn mice pretreated with vehicle ($n = 13$) showed an aversion to the withdrawal-paired environment that was blocked by pretreatment with the CRF_1 receptor antagonist MPZP ($n = 14$; $^*P = 0.0001$). Nicotine-dependent mice that were not experiencing withdrawal and were pretreated with vehicle ($n = 15$) showed a preference for the nicotine-paired environment that was not blocked by MPZP pretreatment ($n = 15$). Nondependent mice given acute nicotine and pretreated with vehicle ($n = 16$) showed an aversion to the nicotine-paired environment that was not blocked by MPZP pretreatment ($n = 15$). Mice with saline minipumps that were pretreated with vehicle ($n = 11$) or MPZP ($n = 12$) showed no motivational response to a novel environment or to MPZP. Data represent mean ± s.e.m. (**c**) Schematic of the aVTA showing placements of the intra-aVTA cannulas (bregma –2.92 mm). (**d**) Schematic of the pVTA showing placements of the intra-pVTA cannulas (bregma –3.40 mm). (**e**) Nicotine-dependent and nicotine-withdrawn mice implanted with cannulas in the pVTA that were given vehicle ($n = 11$) showed an aversive motivational response to the withdrawal-paired environment that was blocked in mice that received intra-pVTA CRF_1 receptor antagonist MPZP ($n = 10$; $^*P = 0.0001$). Dependent and withdrawn mice implanted with aVTA cannulas that were given vehicle ($n = 10$) or MPZP ($n = 12$) showed nicotine withdrawal aversions. Nondependent mice with pVTA cannulas that were pretreated with vehicle ($n = 8$) or MPZP ($n = 10$) and acute nicotine showed an aversive motivational response to the nicotine-paired environment. Control mice implanted with saline minipumps and pVTA cannulas that received vehicle ($n = 12$) or MPZP ($n = 11$) showed no motivational response to a novel environment or to MPZP. Data represent mean ± s.e.m.

To further evaluate the specificity of this effect, we tested the effect of CRF_1 receptor antagonism on the conditioned avoidance response to an acute aversive dose of nicotine[14]. Nondependent mice given acute nicotine and pretreated with saline showed a conditioned place aversion to the nicotine-paired environment that was not blocked by MPZP pretreatment ($P = 0.9228$), which was similar to the results obtained using viral vector–mediated *Crh* mRNA silencing. Mice treated with chronic saline and pretreated with vehicle or MPZP showed no motivational response to a novel environment or to MPZP ($P = 0.8697$), confirming the specificity of these results. These results demonstrate that activation of CRF_1 receptors is selectively required to mediate the aversive motivational response to nicotine withdrawal in dependent mice but not the aversive (in nondependent mice) or rewarding (in dependent mice) motivational effects of nicotine.

To test whether activation of CRF_1 receptors specifically in the pVTA mediates the conditioned aversive motivational response to nicotine withdrawal, we measured place conditioning in separate groups of mice after infusion, before conditioning, of MPZP (0.14 ng/0.3 µl) or vehicle in the aVTA (**Fig. 8c**) and pVTA (**Fig. 8d**). A two-way ANOVA revealed a significant interaction between treatment and nicotine history ($F_{3,76} = 3.351$, $P = 0.0233$; **Fig. 8e**). Nicotine-dependent mice that were in withdrawal and pretreated with vehicle showed an aversive response to the withdrawal-paired environment that was blocked in withdrawn mice pretreated with intra-pVTA MPZP ($P = 0.0063$). However, the ability of MPZP to block nicotine withdrawal aversions was not observed when the CRF antagonist was infused into the aVTA ($P = 0.7108$). These results demonstrate that CRF_1 receptor activation specifically in the pVTA is necessary for the acquisition of the aversive motivational response to nicotine withdrawal in dependent mice. Like mice that received systemic MPZP or the AAV2-shCRH, mice in a nondependent motivational state that received intra-pVTA MPZP or vehicle before acute nicotine administration showed a conditioned avoidance to the acute nicotine-paired environment ($P = 0.7323$). Intra-VTA MPZP had no motivational effects on its own, such that mice implanted with saline minipumps showed neither a preference nor aversion to a MPZP-paired environment ($P = 0.8996$).

DISCUSSION

This report identifies a population of DA neurons in the VTA that expresses CRF in both rodents and humans. Chronic exposure to nicotine increased *Crh* mRNA in the pVTA, and this was associated with a depletion of CRF peptide in VTA and IPN neuropils and blocked nicotine-induced activation of GABAergic input onto DA neurons. Downregulation of *Crh* mRNA in the pVTA restored GABAergic control over DA neurons and prevented the motivational effects of nicotine withdrawal as measured by conditioned place aversion, anxiety-like behavior and escalated nicotine self-administration. Pharmacological testing further demonstrated that the motivational effects of nicotine withdrawal were mediated by activation of CRF_1 receptors in the pVTA.

The detection of CRF neurons in the brain can be very challenging. To confirm the existence of this population of CRF neurons in the VTA, we used a variety of complementary approaches: RT-PCR, radioactive and chromogenic ISH, immunohistochemistry, and fluorescence ISH combined with immunohistochemistry. These techniques revealed direct evidence of CRF neurons in the VTA in rodents and humans. To further confirm the existence of CRF neurons in the VTA, we used several controls, including RT-PCR of housekeeping genes, CRF immunodensity in the aVTA and ISH for urocortin, a member of the CRF family that is structurally related to CRF. Confirming the specificity of the present results, housekeeping genes were not upregulated, CRF immunodensity was altered in the pVTA and IPN but not aVTA, and urocortin-positive neurons were not observed in the pVTA.

TH immunohistochemistry combined with *CRH* ISH showed that most CRF-positive neurons (95% in mice and 98% in humans) also expressed TH, a marker of DA neurons. CRF neurons were distributed bilaterally in the VTA, with the highest number observed in the pVTA in the region dorsal to the IPN. The increase in *Crh* mRNA in nicotine- relative to saline-treated mice was associated with the depletion of CRF in IPN and pVTA neuropils (but not aVTA), suggesting

that the increase in *Crh* mRNA in the VTA was associated with increased CRF release in the pVTA and IPN. Virally mediated *Crh* mRNA downregulation and pharmacological blockade of CRF_1 receptors in the pVTA confirmed the physiological function of increased VTA *Crh* mRNA, CRH release and CRF_1 receptor activation in nicotine-dependent mice.

These results suggest that VTA CRF neurons may release CRF through axons in the IPN and through both axons and dendrites in the pVTA to act as autocrine and paracrine signals[30]. Indeed, unlike classic neurotransmitters, neuropeptides are not only found in axons but also found abundantly in dendrites[31]. CRF specifically is found in dendrites associated with endomembranes and large dense-core vesicles[32], and CRF immunoreactivity has been observed both in axon terminals and dendrites in the VTA[17]. Many groups have attempted to measure CRF in the VTA in rats but failed because of the low concentration, high degradation rate, and low stability and recovery of CRF using microdialysis. The only report of CRF microdialysis in the VTA has not been replicated, and it involved intense footshock stress[33]. New techniques are attempting to use cell-based neurotransmitter fluorescent engineered reporters to reliably measure physiological CRF levels, but these methods are still in their initial stages of development.

The decreased CRF immunodensity in the CeA is in accordance with previous reports showing increased CRF release[27] and reduction of negative emotional states after blockade of CRF_1 receptors in the CeA[34]. The lack of increased *Crh* mRNA in the CeA suggests that the VTA and CeA CRF neurons may be upregulated at different time points. Recent reports showing increased *Crh* mRNA in the CeA 16–24 h into withdrawal[35,36] may explain why an increase was not observed 8 h into withdrawal in the present study. Taken together, these studies demonstrate that blocking the CRF-CRF_1 system in the CeA or VTA is sufficient to prevent the negative emotional states of nicotine withdrawal.

In addition to the upregulation of *Crh* mRNA in VTA DA neurons, chronic nicotine dysregulated GABA-DA synapses, as demonstrated by the loss of inhibitory responses (sIPSCs) to acute nicotine in VTA DA neurons in dependent mice. Virally mediated downregulation of *Crh* mRNA in the pVTA abolished the effect of chronic nicotine on GABA-DA synapses and prevented the motivational effect of withdrawal as measured by conditioned place aversion, anxiety-like behavior, and escalated nicotine self-administration after abstinence. These findings may explain why nicotine dependence *in vivo* decreases in tonic dopaminergic activity in the VTA[15] and DA release in the nucleus accumbens[37], whereas acute CRF_1 receptor antagonism increases tonic DA activity[38]. These findings also may provide a mechanism for observed decreases in accumbal DA release in response to rewards after CRF administration in the VTA[9], the decreased phasic dopamine release observed in cocaine-dependent rats[39] and the decreased prefrontal dopamine metabolism after intra-VTA CRF administration[40]. Indeed, while pharmacological and optogenetic activation of VTA GABA neurons produces robust inhibition of DA neurons[41,42], transient physiological activation of GABAergic input onto DA neurons is required for DA firing[22] because transient GABAergic inputs promote rebound firing in DA neurons. Taken together, these results demonstrate that the activation of a CRF-CRF_1 system in the pVTA may dysregulate transient GABAergic inputs that are critical for dopaminergic firing. Similar effects of CRF on GABAergic input have been observed in the CeA[43].

Increasing evidence suggests that a neurobiological switch occurs in the VTA during the transition from nondependent to drug-dependent motivational states[15,44–46], suggesting that the effect of CRF_1 receptor activation in dependent versus nondependent animals may be opposite. Our results showed a specific role for CRF in the pVTA in mediating the aversive response to nicotine withdrawal in dependent mice but not to acute nicotine in nondependent mice. The specific effect on nicotine intake in long-access but not short-access rats is consistent with this hypothesis, demonstrating that the recruitment of VTA CRF/DA neurons contributes to the development of nicotine dependence. The present results do not exclude the possibility that the expression of CRF in DA neurons alters plasticity in non-DA neurons and circuits in the VTA that may also alter DA function and have motivational significance[46,47]. However, taken with previous results demonstrating that nicotine withdrawal is signaled by a specific pattern of tonic VTA dopaminergic activity[15] and that activation of CRF_1 receptors can mediate changes in VTA DA neuron population activity[38], the present results suggest that chronic nicotine leads to an upregulation of CRF in pVTA DA neurons that is released onto VTA CRF_1 receptors to mediate the aversive motivational effects of nicotine withdrawal. Future studies are necessary to directly test this hypothesis for nicotine and other drugs of abuse.

The transition to drug dependence and drug addiction has been hypothesized to be driven and maintained by two relatively independent systems: downregulation of DA function in the VTA, a within-system neuroadaptation that leads to a reward deficit disorder[48], and upregulation of CRF function, a between-systems neuroadaptation that leads to a stress surfeit disorder[49]. Here we identify a population of CRF neurons in the core of the brain incentive salience and reward system in DA neurons of the pVTA, and show that upregulation of *Crh* mRNA and activation of CRF_1 receptors locally in the pVTA occur after the induction of nicotine dependence and are required for the aversive motivational effects of nicotine withdrawal. This within-system neuroadaptation links the brain reward and stress systems in the same neurobiological substrate, providing evidence that DA and CRF interact in the VTA to mediate the aversive motivational effects of nicotine withdrawal during dependence.

METHODS

Methods and any associated references are available in the online version of the paper.

Note: Any Supplementary Information and Source Data files are available in the online version of the paper.

ACKNOWLEDGMENTS

The authors thank M. Brennan, B. Takabe, C. Arias and the University of Toronto Division of Comparative Medicine staff for technical assistance and M. Arends for editorial assistance. The authors would also like to thank R. Nagra and J. Riehl and the UCLA Brain Bank (The Human Brain and Spinal Fluid Resource Center) for providing the human samples. This work was supported by the Canadian Institutes of Health Research, US National Institute on Drug Abuse (DA023597, DA035371 and DA031566), US National Institute on Alcohol Abuse and Alcoholism (AA021491, AA015566, F32 AA020430, AA006420, AA016658, AA021667 and INIA AA013498), Tobacco-Related Disease Research Program (12RT-0099), US National Institute of Diabetes and Digestive and Kidney Diseases (DK026741) and the Clayton Medical Research Foundation.

AUTHOR CONTRIBUTIONS

T.E.G. and O.G. designed the experiments. T.E.G., H.V.-P., M.C., J.E.S. and G.M.-B. performed minipump, cannulation and viral vector surgeries. M.R. and M.A.H. performed the electrophysiology experiments. T.E.G. performed place conditioning and open field testing. A.C. performed self-administration experiments. C.C., L.A.T. and P.E.S. performed ISH. C.C. and E.C. performed double ISH and immunohistochemistry. T.E.G., V.R.-C., P.P.S., A.R.T. and L.C. performed molecular studies. J.F. and E.C. performed immunohistochemistry. C.C., P.K. and B.L.K. supplied viral vectors. T.E.G. and O.G. analyzed the data. T.E.G., C.C., G.F.K., D.v.d.K. and O.G. wrote the paper. All of the authors discussed the results and read the paper.

COMPETING FINANCIAL INTERESTS
The authors declare no competing financial interests.

1. Volkow, N.D., Fowler, J.S., Wang, G.J., Baler, R. & Telang, F. Imaging dopamine's role in drug abuse and addiction. *Neuropharmacology* **56** (suppl. 1), 3–8 (2009).
2. Koob, G.F. & Le Moal, M. Addiction and the brain antireward system. *Annu. Rev. Psychol.* **59**, 29–53 (2008).
3. Koob, G.F. & Bloom, F.E. Cellular and molecular mechanisms of drug dependence. *Science* **242**, 715–723 (1988).
4. Koob, G.F. & Volkow, N.D. Neurocircuitry of addiction. *Neuropsychopharmacology* **35**, 217–238 (2010).
5. Sarnyai, Z., Shaham, Y. & Heinrichs, S.C. The role of corticotropin-releasing factor in drug addiction. *Pharmacol. Rev.* **53**, 209–243 (2001).
6. Picciotto, M.R. & Kenny, P.J. Molecular mechanisms underlying behaviors related to nicotine addiction. *Cold Spring Harb. Perspect. Med.* **3**, a012112 (2013).
7. Boyson, C.O., Miguel, T.T., Quadros, I.M., Debold, J.F. & Miczek, K.A. Prevention of social stress-escalated cocaine self-administration by CRF-R1 antagonist in the rat VTA. *Psychopharmacology (Berl.)* **218**, 257–269 (2011).
8. Hahn, J., Hopf, F.W. & Bonci, A. Chronic cocaine enhances corticotropin-releasing factor-dependent potentiation of excitatory transmission in ventral tegmental area dopamine neurons. *J. Neurosci.* **29**, 6535–6544 (2009).
9. Wanat, M.J., Bonci, A. & Phillips, P.E. CRF acts in the midbrain to attenuate accumbens dopamine release to rewards but not their predictors. *Nat. Neurosci.* **16**, 383–385 (2013).
10. Wang, B., You, Z.B., Rice, K.C. & Wise, R.A. Stress-induced relapse to cocaine seeking: roles for the CRF_2 receptor and CRF-binding protein in the ventral tegmental area of the rat. *Psychopharmacology (Berl.)* **193**, 283–294 (2007).
11. Wang, H.L. & Morales, M. Corticotropin-releasing factor binding protein within the ventral tegmental area is expressed in a subset of dopaminergic neurons. *J. Comp. Neurol.* **509**, 302–318 (2008).
12. Blacktop, J.M. *et al.* Augmented cocaine seeking in response to stress or CRF delivered into the ventral tegmental area following long-access self-administration is mediated by CRF receptor type 1 but not CRF receptor type 2. *J. Neurosci.* **31**, 11396–11403 (2011).
13. Vranjkovic, O., Gasser, P.J., Gerndt, C.H., Baker, D.A. & Mantsch, J.R. Stress-induced cocaine seeking requires a beta-2 adrenergic receptor-regulated pathway from the ventral bed nucleus of the stria terminalis that regulates CRF actions in the ventral tegmental area. *J. Neurosci.* **34**, 12504–12514 (2014).
14. Grieder, T.E. *et al.* Dopaminergic signaling mediates the motivational response underlying the opponent motivational process to chronic but not acute nicotine. *Neuropsychopharmacology* **35**, 943–954 (2010).
15. Grieder, T.E. *et al.* Phasic D1 and tonic D2 dopamine receptor signaling double dissociate the motivational effects of acute nicotine and chronic nicotine withdrawal. *Proc. Natl. Acad. Sci. USA* **109**, 3101–3106 (2012).
16. Swanson, L.W., Sawchenko, P.E., Rivier, J. & Vale, W.W. Organization of ovine corticotropin-releasing factor immunoreactive cells and fibers in the rat brain: an immunohistochemical study. *Neuroendocrinology* **36**, 165–186 (1983).
17. Tagliaferro, P. & Morales, M. Synapses between corticotropin-releasing factor-containing axon terminals and dopaminergic neurons in the ventral tegmental area are predominantly glutamatergic. *J. Comp. Neurol.* **506**, 616–626 (2008).
18. Kozicz, T. *et al.* The Edinger-Westphal nucleus: a historical, structural, and functional perspective on a dichotomous terminology. *J. Comp. Neurol.* **519**, 1413–1434 (2011).
19. Zhao-Shea, R. *et al.* Nicotine-mediated activation of dopaminergic neurons in distinct regions of the ventral tegmental area. *Neuropsychopharmacology* **36**, 1021–1032 (2011).
20. Merlo Pich, E. *et al.* Increase of extracellular corticotropin-releasing factor-like immunoreactivity levels in the amygdala of awake rats during restraint stress and ethanol withdrawal as measured by microdialysis. *J. Neurosci.* **15**, 5439–5447 (1995).
21. Funk, C.K., O'Dell, L.E., Crawford, E.F. & Koob, G.F. Corticotropin-releasing factor within the central nucleus of the amygdala mediates enhanced ethanol self-administration in withdrawn, ethanol-dependent rats. *J. Neurosci.* **26**, 11324–11332 (2006).
22. Tolu, S. *et al.* Co-activation of VTA DA and GABA neurons mediates nicotine reinforcement. *Mol. Psychiatry* **18**, 382–393 (2013).
23. Hnasko, T.S., Hjelmstad, G.O., Fields, H.L. & Edwards, R.H. Ventral tegmental area glutamate neurons: electrophysiological properties and projections. *J. Neurosci.* **32**, 15076–15085 (2012).
24. Nimitvilai, S., Arora, D.S., McElvain, M.A. & Brodie, M.S. Reversal of inhibition of putative dopaminergic neurons of the ventral tegmental area: interaction of GABA(B) and D2 receptors. *Neuroscience* **226**, 29–39 (2012).
25. Doyon, W.M. *et al.* Nicotine decreases ethanol-induced dopamine signaling and increases self-administration via stress hormones. *Neuron* **79**, 530–540 (2013).
26. Mansvelder, H.D., Keath, J.R. & McGehee, D.S. Synaptic mechanisms underlie nicotine-induced excitability of brain reward areas. *Neuron* **33**, 905–919 (2002).
27. George, O. *et al.* CRF–CRF1 system activation mediates withdrawal-induced increases in nicotine self-administration in nicotine-dependent rats. *Proc. Natl. Acad. Sci. USA* **104**, 17198–17203 (2007).
28. Cohen, A. *et al.* Extended access to nicotine leads to a CRF_1 receptor dependent increase in anxiety-like behavior and hyperalgesia in rats. *Addict. Biol.* doi:10.1111/adb.12077 (2013).
29. Cohen, A., Koob, G.F. & George, O. Robust escalation of nicotine intake with extended access to nicotine self-administration and intermittent periods of abstinence. *Neuropsychopharmacology* **37**, 2153–2160 (2012).
30. Ludwig, M. & Leng, G. Dendritic peptide release and peptide-dependent behaviours. *Nat. Rev. Neurosci.* **7**, 126–136 (2006).
31. Son, S.J. *et al.* Dendritic peptide release mediates interpopulation crosstalk between neurosecretory and preautonomic networks. *Neuron* **78**, 1036–1049 (2013).
32. Treweek, J.B., Jaferi, A., Colago, E.E., Zhou, P. & Pickel, V.M. Electron microscopic localization of corticotropin-releasing factor (CRF) and CRF receptor in rat and mouse central nucleus of the amygdala. *J. Comp. Neurol.* **512**, 323–335 (2009).
33. Wang, B. *et al.* Cocaine experience establishes control of midbrain glutamate and dopamine by corticotropin-releasing factor: a role in stress-induced relapse to drug seeking. *J. Neurosci.* **25**, 5389–5396 (2005).
34. Marcinkiewcz, C.A. *et al.* Corticotropin-releasing factor within the central nucleus of the amygdala and the nucleus accumbens shell mediates the negative affective state of nicotine withdrawal in rats. *Neuropsychopharmacology* **34**, 1743–1752 (2009).
35. Baiamonte, B.A. *et al.* Nicotine dependence produces hyperalgesia: role of corticotropin-releasing factor-1 receptors (CRF1Rs) in the central amygdala (CeA). *Neuropharmacology* **77**, 217–223 (2014).
36. Torres, O.V., Gentil, L.G., Natividad, L.A., Carcoba, L.M. & O'Dell, L.E. Behavioral, biochemical, and molecular indices of stress are enhanced in female versus male rats experiencing nicotine withdrawal. *Front. Psychiatry* **4**, 38 (2013).
37. Zhang, L., Dong, Y., Doyon, W.M. & Dani, J.A. Withdrawal from chronic nicotine exposure alters dopamine signaling dynamics in the nucleus accumbens. *Biol. Psychiatry* **71**, 184–191 (2012).
38. Lodge, D.J. & Grace, A.A. Acute and chronic corticotropin-releasing factor 1 receptor blockade inhibits cocaine-induced dopamine release: correlation with dopamine neuron activity. *J. Pharmacol. Exp. Ther.* **314**, 201–206 (2005).
39. Willuhn, I., Burgeno, L.M., Groblewski, P.A. & Phillips, P.E. Excessive cocaine use results from decreased phasic dopamine signaling in the striatum. *Nat. Neurosci.* **17**, 704–709 (2014).
40. Kalivas, P.W., Duffy, P. & Latimer, L.G. Neurochemical and behavioral effects of corticotropin-releasing factor in the ventral tegmental area of the rat. *J. Pharmacol. Exp. Ther.* **242**, 757–763 (1987).
41. van Zessen, R., Phillips, J.L., Budygin, E.A. & Stuber, G.D. Activation of VTA GABA neurons disrupts reward consumption. *Neuron* **73**, 1184–1194 (2012).
42. Tan, K.R. *et al.* GABA neurons of the VTA drive conditioned place aversion. *Neuron* **73**, 1173–1183 (2012).
43. Roberto, M. *et al.* Corticotropin releasing factor-induced amygdala gamma-aminobutyric acid release plays a key role in alcohol dependence. *Biol. Psychiatry* **67**, 831–839 (2010).
44. Nader, K. & van der Kooy, D. Deprivation state switches the neurobiological substrates mediating opiate reward in the ventral tegmental area. *J. Neurosci.* **17**, 383–390 (1997).
45. Vargas-Perez, H. *et al.* Ventral tegmental area BDNF induces an opiate-dependent like reward state in naive rats. *Science* **324**, 1732–1734 (2009).
46. Laviolette, S.R., Alexson, T.O. & van der Kooy, D. Lesions of the tegmental pedunculopontine nucleus block the rewarding effects and reveal the aversive effects of nicotine in the ventral tegmental area. *J. Neurosci.* **22**, 8653–8660 (2002).
47. Steffensen, S.C. *et al.* Contingent and non-contingent effects of heroin on mu-opioid receptor-containing ventral tegmental area GABA neurons. *Exp. Neurol.* **202**, 139–151 (2006).
48. Volkow, N.D., Fowler, J.S., Wang, G.J., Swanson, J.M. & Telang, F. Dopamine in drug abuse and addiction: results of imaging studies and treatment implications. *Arch. Neurol.* **64**, 1575–1579 (2007).
49. Koob, G.F. *et al.* Addiction as a stress surfeit disorder. *Neuropharmacology* **76** (pt. B), 370–382 (2014).
50. Paxinos, G. & Franklin, K.B.J. *The Mouse Brain in Stereotaxic Coordinates* (Academic, San Diego, 1997).

ONLINE METHODS

Animals. All animal use procedures were approved by the University of Toronto Animal Care Committee in accordance with the Canadian Council on Animal Care guidelines and The Scripps Research Institute Institutional Animal Care and Use Committee, and were in accordance with US National Institutes of Health guidelines. Adult male C57BL/6 mice (2–4 months) (Charles River, Montreal, Canada, or Hollister, CA, USA) were housed in a temperature-controlled room with lights on from 7:00 a.m. to 7:00 p.m. Adult male Wistar rats (2–4 months) (Charles River, Hollister, CA, USA) were housed in a temperature-controlled room with lights on from 8:00 p.m. to 8:00 a.m. Animals were grouped 2–4 per cage. Behavioral testing was performed during the dark cycle.

Drugs. Nicotine hydrogen tartrate salt (Sigma-Aldrich, Ontario, Canada) was dissolved in saline, pH 7.0 ± 0.4, and administered via osmotic minipumps (chronic nicotine, 7 mg kg^{-1} d^{-1}, minipump model 1002, Alzet, Cupertino, CA, USA) or subcutaneous injection (acute nicotine, 1.75 mg kg^{-1}). Nicotine-dependent and nicotine-withdrawn mice had their minipumps removed 8 h before experimentation, a time that corresponds to peak motivational withdrawal[14]. The CRF_1 receptor antagonist MPZP[51] was synthesized at The Scripps Research Institute, dissolved in (2-hydroxypropyl)-β-cyclodextrin (HBC) and administered subcutaneously 20 min before conditioning or at a concentration of 0.14 μg/0.3 μl over 10 min for intra-VTA infusions.

Viral vector production. shRNA-encoding AAV2 vectors that target the *Crh* transcript were generated using the same procedure as described in ref. 52. A shRNA sequence (shCRH, sense strand 5′-GGATCTCACCTTCCACCTTCT-3′) predicted to have high silencing efficiency was selected using Block-iT RNAi Designer (Life Technologies, Carlsbad, CA, USA). A universal scrambled shRNA with no homology to any transcripts was used as a control (shSCR, sense strand 5′-GCGCTTAGCTGTAGGATTC-3′). An AAV2 shuttle plasmid that encodes shCRH or shSCR downstream of the mU6 promoter and enhanced green fluorescent protein (EGFP) under the control of the cytomegalovirus (CMV) promoter 3′-flanked by a β-globin intron was generated using Invitrogen Gateway technology. Helper-free AAV2 particles were produced by the triple transfection of AAV-293 cells (Agilent Technologies, Santa Clara, CA, USA) with the AAV2 shuttle plasmid described above, a plasmid that contains AAV2 rep and cap genes, and a plasmid that encodes the adenovirus helper functions. Two days later, cells were collected and lysed by three freeze-thaw cycles and the lysate was treated with benzonase and clarified by centrifugation. Viral vectors were purified by iodixanol-gradient ultracentrifugation[53], followed by dialysis against Dulbecco phosphate-buffered saline (PBS) and concentration using centrifugal filter units (Millipore, Billerica, MA, USA). Genomic units (GU) were quantified by RT-PCR. The titers were 4.5×10^{11}–6.6×10^{11} GU/ml.

Viral vector and drug infusion. Mice and rats were anesthetized (1–5% isoflurane in oxygen mixture) and placed in a Kopf stereotaxic instrument. Double cannulas (Plastics One, Roanoke, VA, USA) were inserted bilaterally above the left and right VTA. The coordinates used were relative to bregma and from skull surface, as follows. Mouse coordinates: aVTA (anterior/posterior [AP], −3.3 mm; dorsal/ventral [DV], −4.4 mm; medial/lateral [ML], ± 0.5 mm); pVTA (AP, −3.6 mm; DV, −4.4 mm; ML, ± 0.5 mm). Each rat received two injections of the virus directed at different AP positions of the VTA. Rat coordinates: AP, −5.4 and −5.8 mm; ML, ± 0.7 mm; DV, −8.2 mm. Each mouse received 0.75 μl/side and each rat received 1 μl/side of either the AAV2-shCRH or AAV2-shSCR at an infusion rate of 0.1 μl/min using injectors that protruded 1 mm beyond the cannula (for mice) or 2 mm beyond the cannula (for rats). The injectors were left in place for 10 more minutes to ensure adequate diffusion of the solution. Infusions were delivered via polyethylene tubing (PE 20) that was connected to a Hamilton 10-μl syringe.

For intra-VTA MPZP infusion, dummy cannulas were secured in the injection cannulas by dust caps, and the animals were allowed to recover for 1 week before drug infusion and conditioning. On conditioning days, the dust cap and dummy cannulas were removed and replaced with injector cannulas. Mice were lightly restrained and infused with 0.14 μg in 0.3 μl MPZP or 20% HBC (control solution) over 1 min. After the behavioral experiments were completed, the mice were sacrificed and perfused, and cannula placement was verified by cresyl violet staining. Sixteen of 100 mice were excluded owing to incorrect cannula placements.

Real-time RT-PCR. RNA was isolated using a Qiagen RNeasy extraction kit with DNase to remove genomic DNA contamination and a specified amount of RNA was reverse-transcribed using SuperScript III (Invitrogen, Foster City, CA, USA) to generate cDNAs. Quantitative real-time PCR was performed using Taqman Gene Expression Assays for *Crh* (Mm01293920_s1) in a 7900HT Fast RT-PCR System (both from Life Technologies, Carlsbad, CA, USA). Quantification was performed using the ΔC_t method with *Gapdh* as an endogenous control. For single-cell RT-PCR analysis, single cells were collected from AAV2-shCRH- or AAV2-shSCR-injected brain slices by aspiration of neuronal cytoplasm immediately after electrophysiological recordings, and processed with the Picopure RNA isolation kit (Life Technologies, Carlsbad, CA, USA) for RNA isolation and reverse transcription (RT) using the iScript cDNA synthesis kit (Bio-Rad, Hercules, CA, USA). The cDNA obtained from single neurons was subjected to preamplification for 20 cycles, followed by real-time RT-PCR to detect the expression of TH with forward (5′-ACTGCTTCTCAACCACATCTT-3′) and reverse (5′-GGGTAGAATACAGCATGAAGGG-3′) primers using the SSO Advanced SYBR Green Supermix (Bio-Rad, Hercules, CA, USA) according to manufacturer's protocol.

Radioactive *in situ* hybridization. Mice were anesthetized with chloral hydrate (350 mg kg^{-1}, i.p.) and perfused via the ascending aorta with 0.9% saline followed by ice-cold 4% paraformaldehyde in 0.1 M borate buffer, pH 9.5. The brains were removed, postfixed for 3 h, and cryoprotected in 20% sucrose in 0.1 M phosphate buffer overnight at 4 °C. Five one-in-four series of 30-μm-thick frozen coronal sections were cut, collected, and stored in 30% ethylene glycol and 20% glycerol in 0.1 M phosphate buffer at −20 °C until processing. *In situ* hybridization was performed using ^{35}S-labeled sense (control) and antisense cRNA probes labeled to similar specific activities using a full-length (1.2 kb) probe for the mRNA that encodes CRF (1.2 kb; K. Mayo, Northwestern University, Evanston, IL, USA). Sections were mounted on Superfrost Plus slides and dried under vacuum overnight. They were postfixed with 10% formalin for 30 min at room temperature, digested with 10 μg/ml proteinase K for 15 min at 37 °C and acetylated for 10 min. The probes were labeled to specific activities of 1×10^9–3×10^9 c.p.m./μg and applied to the slides at concentrations of ~10^7 c.p.m./ml overnight at 56 °C in a solution that contained 50% formamide, 0.3 M NaCl, 10 mM Tris, 1 mM EDTA, 0.05% tRNA, 10 mM dithiothreitol, 1× Denhardt's solution and 10% dextran sulfate, after which they were treated with 20 μg/ml of RNase A for 30 min at 37 °C and washed in 15 mM NaCl/1.5 mM sodium citrate with 50% formamide at 70 °C. The slides were then dehydrated and exposed to X-ray film (Kodak Biomax MR, Eastman Kodak, Rochester, NY, USA) for 18 h. They were coated with Kodak NTB-2 liquid emulsion and exposed at 4 °C for 3–4 weeks as determined by the strength of the signal on the film. The slides were developed with Kodak D-19 and fixed with Kodak rapid fixer. One series of sections that adjoined those used for analysis was stained with thionin to facilitate the accurate localization of hybridization signals. The experimenters were blind to the experimental history of the animals.

Densitometry. The semiquantitative densitometric analysis of hybridization signals for *Crh* mRNA was performed on emulsion-dipped slides. Photomicrographs were captured using a Leica light microscope with a Hamamatsu Orca charge-coupled-device camera through OpenLab software (version 3.1.5) and analyzed using ImageJ software. The optical densities of hybridization signals were determined under dark-field illumination at 400× magnification with a circular region of interest (ROI) of 20 μm diameter that was placed over individual neurons. The size of the ROI was chosen on the basis of the average diameter of TH-immunoreactive neurons in the pVTA. The sections were analyzed at regular 120-μm intervals across the pVTA. Optical densities were corrected for the average background signal that was determined by sampling 20 cell-sized areas per section in nonsignal areas adjacent to the pVTA. Optical density values are expressed in gray scale values of 1 to 256, corresponding to a gradation from low to high absorbance, respectively. Neurons on both sides of the brain were pooled for analysis to calculate the animal mean. Animal means were then grouped according to virus treatment, averaged and statistically analyzed. The experimenters were blind to the experimental history of the animals during densitometry analysis.

Immunohistochemistry. Mice were anesthetized with 3% halothane, preperfused transcardially with a solution of 0.5 ml heparin/100 ml saline for

1–2 min and then perfused with a solution of 4% paraformaldehyde in 0.1 M phosphate buffer, pH 7. The experimenters were blind to the drug history of the animals. The brains were removed from the skull, postfixed at 4 °C in the perfusate solution for 6–18 h, rinsed in several changes of PBS containing 20% sucrose and stored at 4 °C in fresh 20% sucrose/PBS that contained 0.1% sodium azide. Coronal cryostat sections (40 µm) were obtained using a Reichert Jung cryostat. The sections were collected in strict anatomical order in a one-in-four series and stored at 4 °C in PBS 0.1% azide before processing. The sections were incubated free-floating with shaking in multiwell plates, and all incubations were performed at room temperature unless otherwise specified. The samples were incubated for 20 min in 1% hydrogen peroxide/PBS to quench endogenous peroxidases, rinsed several times in PBS and exposed to a blocking solution that contained PBS/Triton X-100 (0.3%), 1 mg/ml bovine serum albumin (BSA) and 5% normal donkey serum (Jackson ImmunoResearch, West Grove, PA, USA) for a minimum of 60 min. The sections were incubated overnight at 4 °C in anti-CRF purified goat polyclonal antibody (sc-1761, Santa Cruz Biotechnology, Santa Cruz, CA, USA) diluted 1:200 in PBS, 0.5% Tween-20 and 5% normal donkey serum. Control sections were incubated in the antibody diluent. Following three rinses of 10 min each in PBS, the sections were incubated in Vector ImmPRESS Goat (Vector Labs, Burlingame, CA, USA) for 1 h, rinsed in PBS as above and reacted with a DAB substrate kit (Vector Labs). The sections were monitored under a microscope to determine the optimal reaction time. The reaction was stopped in PBS. The sections were mounted on coated slides, air dried, dehydrated through a series of ethanol and xylene, and coverslipped with Permount. All brightfield photographs for analysis were taken with a Q Imaging Retiga 2000R color digital camera mounted on a Zeiss Axiophot microscope.

Combined TH immunohistochemistry and *Crh* fluorescence *in situ* hybridization. Mouse brains were snap-frozen using isopentane. Twenty-micrometer cryostat sections were mounted on Superfrost Plus slides. A digoxigenin (DIG)-labeled *Crh* riboprobe was synthesized using a commercial kit (Roche, Indianapolis, IN, USA) from a plasmid containing full-length rat *Crh* cDNA (kind donation from K. Mayo, Northwestern University, Evanston, IL, USA). The sections were postfixed in 4% formaldehyde for 1 min. Following PBS washes, proteins were acetylated in 0.1 M triethanolamine, pH 8.0, and 0.2% acetic acid. Following washes in 2× saline sodium citrate buffer, the sections were dehydrated in a graded ethanol-chloroform series. Prehybridization and hybridization were then performed at 70 °C in a buffer containing 50% formamide, 2× SSC, 5× Denhardt's reagent, 0.5 mg/ml sheared salmon sperm DNA and 0.25 mg/ml yeast total RNA. The probe was diluted in the hybridization buffer (800 ng/ml) and incubated overnight on slides. Post-hybridization washes were performed in 50% formamide, 2× SSC and 0.1% Tween-20. The slides were then blocked for 1 h and incubated with anti-DIG antibody conjugated to alkaline phosphatase (11093274910, Roche; 1:1,000) and anti-TH antibody (AB152, Millipore, Billerica, MA, USA; 1:500) overnight at 4 °C in TNT buffer (0.1 M Tris, pH 7.5, 0.15 M NaCl, 0.1% Tween-20) containing 1% blocking reagent (Roche). A donkey anti-rabbit secondary antibody conjugated to Alexa Fluor 488 (A-21206, Life Technologies, Carlsbad, CA, USA; 1:200, 2 h) was used to reveal the TH signal. Following TNT washes and incubation in 0.1 M Tris-HCl, pH 8, 0.1 M NaCl, 0.01 M $MgCl_2$, HNPP combined with Fast Red TR (Roche) was then used to detect alkaline phosphatase. To enhance the signal, fresh substrate was applied three times for 30 min, and the slides were rinsed in TNT in between. The slides were washed, air dried, and coverslipped with Vectashield HardSet-DAPI (Vector Laboratories, Burlingame, CA, USA). Images were taken using either epifluorescence (Zeiss Axiophot) or confocal microscopy (LaserSharp 2000, version 5.2; 488, 568 and 647 nm emission wavelengths; Bio-Rad, Hercules, CA, USA).

Human brain samples (TH immunohistochemistry and *CRH* chromogenic *in situ* hybridization). Human brain samples (snap-frozen and stored at −80 °C) were obtained from the UCLA Brain Bank. For chromogenic *in situ* hybridization, brain sections were processed as described above for fluorescence *in situ* hybridization, except that slides were incubated with NBT-BCIP (Sigma) as an alkaline phosphatase substrate at room temperature overnight in the dark. Sections were then rinsed in PBS Tween-20 and air-dried.

For double labeling with TH, sections were then fixed in 4% paraformaldehyde/PBS for 15 min, rinsed in PBS, quenched for 20 min in 1% hydrogen peroxide/PBS, rinsed in PBS and blocked for 1 h at room temperature in PBS/TX-100 (0.3%), BSA (1 mg/ml) and 5% normal donkey serum (Jackson). Sections were incubated in rabbit polyclonal TH antibody (1:1,000, Millipore AB152) and diluted in PBS, 0.5% Tween-20 and 5% normal donkey serum overnight at room temperature in a humidity chamber. Following PBS rinses, the sections were incubated in Rabbit ImmPRESS (Vector Labs) for 1–2 h at room temperature. Following PBS rinses, the sections were incubated in either Vector ImmPACT Red (Vector Labs) or DAB substrate (Vector Labs). The reaction was stopped in PBS rinses and the sections were air-dried and coverslipped with DPX.

Brain slice preparation (electrophysiology). Slices that contained the VTA were prepared as described previously[24] from 20 adult male C57BL/6 mice subjected to brief anesthesia (3–5% isoflurane) followed by rapid decapitation and removal of the brain to an ice-cold high-sucrose solution (pH 7.3–7.4) that contained 206.0 mM sucrose, 2.5 mM KCl, 0.5 mM $CaCl_2$, 7.0 mM $MgCl_2$, 1.2 mM NaH_2PO_4, 26 mM $NaHCO_3$, 5.0 mM glucose and 5 mM HEPES. The brains were cut into transverse sections (300 µm) on a vibrating microtome (Leica VT1000S, Leica Microsystems, Buffalo Grove, IL, USA) and placed in an oxygenated (95% O_2/5% CO_2) artificial cerebrospinal fluid (aCSF) solution composed of the following: 120 mM NaCl, 2.5 mM KCl, 5 mM EGTA, 2.0 mM $CaCl_2$, 1.0 mM $MgCl_2$, 1.2 mM NaH_2PO_4, 26 mM $NaHCO_3$, 1.75 mM glucose and 5 mM HEPES. The slices were incubated in this solution for 30 min at 35–37 °C, followed by 30 min equilibration at room temperature (21–22 °C). Following equilibration, a single slice was transferred to a recording chamber mounted on the stage of an upright microscope (Olympus BX50WI).

Electrophysiological recording. Neurons were visualized on an upright microscope (Olympus BX50WI) with infrared differential interference contrast optics and an EXi Aqua camera (QImaging, Surrey, BC, Canada). To avoid photolytic damage, initial exposure to episcopic fluorescence illumination was brief (<2 s). Fluorescence was detected using an X-Cite 120Q fluorescence illumination system (Lumen Dynamics, Mississauga, Ontario, Canada) and images were captured using QCapture software (QImaging). In all cases, the experimenter was blind to the nature of the viral vector injected into the mouse before experimental recording and data analysis. Whole-cell (voltage- and current-clamp) recordings were made with patch pipettes (3–5 MΩ; Warner Instruments) coupled to a Multiclamp 700B amplifier (Molecular Devices, Sunnyvale, CA, USA), low-pass filtered at 2–5 kHz, digitized (Digidata 1440A; Axon Instruments) and stored on a computer using pClamp 10 software (Axon Instruments). Series resistance was typically <10 MΩ and continuously monitored with a hyperpolarizing 10 mV pulse. The intracellular solution used for recordings was composed of 145 mM KCl, 5 mM EGTA, 5 mM $MgCl_2$, 10 mM HEPES, 2 mM Na-ATP and 0.2 mM Na-GTP. To isolate only the inhibitory currents mediated by $GABA_A$ receptors, recordings (V_{hold} = −60 mV) were performed in the presence of the glutamate receptor blockers 6,7-dinitroquinoxaline-2,3-dione (DNQX; 20 µM) and DL-2-amino-5-phosphonovalerate (AP-5; 50 µM) and the $GABA_B$ receptor antagonist CGP55845A (1 µM). Owing to rapidly desensitizing effects, nicotine was bath applied for 5–7 min but the period of analysis was restricted to 2 min after full wash-in. The frequency, amplitude and decay of spontaneous inhibitory postsynaptic currents (sIPSCs) were analyzed and visually confirmed using semiautomated, threshold-based mini-detection software (Mini Analysis, Synaptosoft Inc.). We determined averages of IPSC characteristics from baseline and experimental drug conditions containing a minimum of 60 events (time period of analysis varied as a product of individual event frequency), and we determined decay kinetics using exponential curve fittings, which are reported as decay time (ms). All of the detected events were used for event frequency analysis, but superimposed events were eliminated for amplitude and decay kinetic analysis. Action potential characteristics were evaluated using threshold-based event detection analysis in Clampfit 10.2 (Molecular Devices).

Place conditioning. The place conditioning apparatus was obtained from Med Associates (SOF-700RA-25 Two Chamber Place Preference Apparatus; St. Albans, VT, USA). One environment was black with a metal rod floor and the other was white with a wire mesh floor. An intermediate gray area housed a removable partition. Each cage was cleaned between animals, and each group was fully counterbalanced. During preference testing, the dividing partition was removed and

doi:10.1038/nn.3872

the mice were given free access to both environments. A single 10-min preference test session was performed 5 d after the last conditioning day. All place conditioning and testing were performed between 10:00 a.m. and 6:00 p.m.

The nicotine-dependent and nicotine-withdrawn groups of mice were conditioned according to modified place conditioning procedures as described previously[14]. Conditioning occurred only during withdrawal from chronic nicotine so that the motivational effects of withdrawal but not the direct effects of chronic nicotine were paired with the place conditioning environment. Eight hours after minipump removal, when the mouse was experiencing motivational withdrawal from chronic nicotine[14], it was subcutaneously or intracranially pretreated with vehicle (HBC) or MPZP and confined to one of the conditioning environments for 1 h. The difference score for each animal was calculated by subtracting the time spent in the nonpaired environment from the time spent in the withdrawal-paired environment during preference testing.

For nicotine-dependent mice (not withdrawn), conditioning occurred only during exposure to chronic nicotine so that the motivational effects of chronic nicotine in a dependent animal were paired with the place conditioning environment. The mice were subcutaneously pretreated with vehicle (20% HBC) or MPZP (20 mg kg^{-1}) and confined to one of the conditioning environments for 1 h. The difference score for each animal was calculated by subtracting the time spent in the nonpaired environment from the time spent in the nicotine-paired environment during preference testing.

For the acute nicotine experiments, previously drug-naive mice were subcutaneously or intracranially pretreated with 20% HBC or MPZP, given a subcutaneous injection of 1.75 mg kg^{-1} nicotine or saline, and immediately confined to one of the conditioning environments for 1 h. The next day, the mouse was pretreated again with HBC or MPZP, given acute saline or nicotine, and confined to the other environment. The difference score for each animal was calculated by subtracting the time spent in the saline-paired environment from the time spent in the nicotine-paired environment. In all cases, the experimenter was blind to the previous drug and/or viral vector treatment.

Open field testing. Mice were placed in the center of a gray box measuring 41 × 41 × 38 cm for 5 min. The room was dark, with the open field testing box illuminated by a soft red light. Locomotor activity and time spent in the center square area of the box were recorded by a video camera and calculated by the monitoring program (Ethovision XT, Noldus; Leesburg, VA, USA). The experimenter was blind to the mouse's previous drug and viral vector history. The test box was cleaned with 70% alcohol between each mouse.

Nicotine self-administration. Two weeks after infusion, rats were implanted with intravenous catheters in the jugular vein under isoflurane anesthesia as described previously[29]. Detailed procedures for the escalation of nicotine self-administration have been described previously[29]. Briefly, 3 weeks after the injection of viral vectors in the VTA, rats were trained to nosepoke for food and water in their self-administration chambers in 21-h sessions but were not food-trained to respond for the lever that was associated with nicotine delivery. Subsequently, the active and inactive levers were extended and the rats were allowed to self-administer nicotine (0.03 or 0.0 mg kg^{-1} per 100 µl/1 s, free base, FR1, timeout 20 s) for 10 d (1 h per day). The rats were then allowed daily long-access (LgA; 21 h) nicotine or saline self-administration sessions for 7 consecutive days, followed by 48 h of abstinence and another LgA session to measure abstinence-induced escalation of nicotine intake.

Statistical analysis. The behavioral data were analyzed with Statistica software using a one- or two-way ANOVA or Student's *t*-test, as appropriate. In all cases, a normality test and an equal variance test were performed before the ANOVA to ensure its validity. For electrophysiology, statistical analysis was performed using Prism 5.02 software (GraphPad, San Diego, CA). Groups were analyzed for independent significance using a one-sample *t*-test and compared using an unpaired *t*-test for comparisons between two groups and a one-way ANOVA for comparisons between three or more groups. All experiments and analyses were performed by experimenters who were blind to the treatments, and the animals' order of treatment was randomized. No statistical methods were used to predetermine sample sizes, but our sample sizes are similar to those reported in previous publications[13,25,37,39]. Different numbers of animals between groups and between the beginning and end of the study are a result of the loss of data due to improper cannula placement, improper brain perfusion, damaged brain samples or computer failure during testing. For all analyses, Bonferroni *post hoc* tests were used when appropriate. All data are expressed as mean ± s.e.m.

A **Supplementary Methods Checklist** is available.

51. Richardson, H.N. *et al.* MPZP: a novel small molecule corticotropin-releasing factor type 1 receptor (CRF1) antagonist. *Pharmacol. Biochem. Behav.* **88**, 497–510 (2008).
52. Darcq, E. *et al.* RSK2 signaling in brain habenula contributes to place aversion learning. *Learn. Mem.* **18**, 574–578 (2011).
53. Zolotukhin, S. *et al.* Production and purification of serotype 1, 2, and 5 recombinant adeno-associated viral vectors. *Methods* **28**, 158–167 (2002).